Principles for designing sputtering-based strategies for high-rate synthesis of dense and hard hydrogenated amorphous carbon thin films

Asim Aijaz, Kostas Sarakinos, Mohsin Raza, Jens Jensen and Ulf Helmersson

Journal Article

Original Publication:

Asim Aijaz, Kostas Sarakinos, Mohsin Raza, Jens Jensen and Ulf Helmersson, Principles for designing sputtering-based strategies for high-rate synthesis of dense and hard hydrogenated amorphous carbon thin films, Diamond and related materials, 2014. 44, pp.117-122.
http://dx.doi.org/10.1016/j.diamond.2014.02.014

Principles for designing sputtering-based strategies for high-rate synthesis of dense and hard hydrogenated amorphous carbon thin films

Asim Aijaz*, Kostas Sarakinos, Mohsin Raza[1], Jens Jensen and Ulf Helmersson

IFM-Materials Physics, Linköping University, SE-581 83 Linköping, Sweden.

*Corresponding author. E-mail: asim@ifm.liu.se

Tel: +46-13-282629

[1]Currently at: Chimie des Interactions Plasma-Surface (ChIPS)

University of Mons

23 Place du Parc, 7000 Mons, Belgium.

Abstract

In the present study we contribute to the understanding that is required for designing sputtering-based routes for high rate synthesis of hard and dense hydrogenated amorphous carbon (a-C:H) films. We compile and implement a strategy for synthesis of a-C:H thin films that entails coupling a hydrocarbon gas (acetylene) with high density discharges generated by the superposition of high power impulse magnetron sputtering (HiPIMS) and direct current magnetron sputtering (DCMS). Appropriate control of discharge density (by tuning HiPIMS/DCMS power ratio), gas phase composition and energy of the ionized depositing species leads to a route capable of providing ten-fold increase in the deposition rate of a-C film growth compared to HiPIMS Ar discharge (Aijaz *et al.* Diamond and Related Materials 23 (2012) 1). This is achieved without significant incorporation of H (< 10 %) and with relatively high hardness (> 25 GPa) and mass density (~2.32 g/cm^3). Using our experimental data together with Monte-Carlo computer simulations and data from the literature we suggest that: (i) dissociative reactions triggered by the interactions of energetic discharge electrons with hydrocarbon gas molecules is an important additional (to the sputtering cathode) source of film forming species and (ii) film microstructure and film hydrogen content are primarily controlled by interactions of energetic plasma species with surface and sub-surface layers of the growing film.

Key words: diamond-like carbon, hydrogenated amorphous carbon, HiPIMS, HPPMS, PECVD

I. INTRODUCTION

The physical attributes and thus the performance of amorphous carbon (a-C) thin films in technological applications are largely determined by their bonding configuration (i.e., sp^3-to-sp^2 bond ratio), as well as on the amount of hydrogen in the films [1–7]. Bonding configuration and hydrogen content can be, in turn, tailored by controlling the energy and flux of the depositing species [5,6]. An efficient way to achieve this is by using ionized deposition fluxes which can be generated by high plasma density discharges, such as cathodic vacuum arc (CVA) [8,9], pulsed laser deposition (PLD) [10,11], inductively coupled plasma (ICP) [12] and electron cyclotron resonance (ECR) [13] based plasma enhanced chemical vapor deposition (PECVD). Synthesis of a-C using magnetron sputtering-based discharges may be more industrially relevant owing to their conceptual simplicity and scalability. However, these discharges (e.g., direct current and radio frequency magnetron sputtering) are characterized by relatively low plasma densities [14,15] and they are, thus, unable to generate large fluxes of C ions [14]. Using magnetron sputtering based high plasma density discharges such as high power impulse magnetron sputtering (HiPIMS) [15] a higher C ionized fraction, mass density as well as sp^3/sp^2 fraction has been obtained. However these properties are not comparable to those obtained by CVA and PLD [16,17]. In a previous study we addressed this issue by conceiving and implementing a strategy [18] which entailed increase of the electron temperature in high electron density discharge (such as HiPIMS) by using higher ionization potential buffer gas, Ne, instead of Ar. The result was a substantial increase in the ionized fraction of C which facilitated an increase in mass densities of films to levels which are close to those obtained by CVA and PLD [8,10].

Another issue encountered in sputtering-based processes is the relatively low sputtering yield of C and thus growth rates of the deposited a-C films. This drawback can be circumvented by introducing an additional source of C such as by coupling a hydrocarbon precursor gas to the

discharge. The downside of adding a hydrocarbon precursor in the process is the generation of a substantial amount of H [19]. Incorporation of H in the films results in formation of C-H sp^3 bonds which reduces the mass density and C-C bonding in the film thereby impairing the synthesis of high density phases [5,20]. Combination of hydrocarbon gases with high density discharges and the resulting energetic bombardment of the growing film by the abundant ionized species may alter the surface and subsurface conditions facilitating a control over H incorporation. In this work we implement this strategy by coupling C_2H_2 with high density plasma discharges to synthesize a-C:H thin films. High density discharges are generated by superimposing HiPIMS and direct current magnetron sputtering (DCMS) which allows varying plasma densities (by changing HiPIMS power fraction) while maintaining stable operating conditions. Seeking to contribute to the understanding that is required for designing sputtering-based routes for high rate synthesis of hard and dense a-C:H films we study and discuss the effect of energetic bombardment and plasma chemistry on film growth. This is achieved by establishing the relationships between process conditions and film properties (mass density, H content, hardness) and identifying chemical pathways that lead to a-C:H growth. In addition, Monte Carlo based computer simulations [21] are employed to elucidate ion-surface interactions and assess their role on the film growth.

II. EXPERIMENTAL PROCEDURE

A. GENERAL EXPERIMENTAL PROCEDURE

Experiments were performed using a 50 mm in diameter and 3 mm thick C target (purity 99.9%) mounted on an unbalanced magnetron. The magnetron was mounted in a cylindrical shaped stainless steel chamber of height 300 mm and diameter of 420 mm. Prior to depositions, the chamber was evacuated to a base pressure below 2×10^{-4} Pa. Ar gas (purity 99.9997%) mixed with C_2H_2 (purity 99.6%) was used as the process gas. A fraction of 2%

and 5% C_2H_2 was used in the gas mixture for different processes (see section II. B) by varying its partial pressure while the total pressure was kept constant at 2 Pa. Films were deposited on water cooled single crystalline Si (100) substrates placed on a fixed substrate holder at a distance of 60 mm from the surface of the target. The substrates were ultrasonically cleaned using acetone and isopropanol each for 5 min and blown dried using dry nitrogen before they were loaded into the deposition chamber. Prior to depositions, the substrates were plasma etched in a pure Ar ambient at 4 Pa, where the plasma was ignited by applying a negative pulsed bias voltage of 600 V at a repetition rate of 100 kHz to the substrate holder. The power to the cathode was applied using a superposition of DCMS and HiPIMS powers. The DC power was supplied using an MDX 1K DC generator (Advanced Energy) operated in constant power mode. The HiPIMS power was supplied using a pulsing unit (own design) fed by another MDX 1K DC generator operated in constant power mode. In the superposition arrangement, both power sources were connected (in parallel) to the cathode such that the power at the cathode was the sum of the two power feeds. In this arrangement, the pulsed supply was isolated from the DC supply by connecting a diode in series with the DC supply and the cathode. The HiPIMS power was obtained by using pulses with a repetition frequency of 600 Hz and pulse duration of 25 μs resulting in a duty cycle of 1.5%. The discharge parameters, such as cathode voltage and cathode current were monitored and recorded on a Tektronix TDS2004B oscilloscope.

During all film depositions, the incident energy of the depositing species (E_{ion}) was controlled by applying a negative pulsed bias potential to the substrate with an operation frequency of 100 kHz. The absolute values of the bias potentials are represented by U_b. The range of the bias potential was chosen from floating potential, V_{fl} (~ –15 V) to –300 V. The mass density and the thickness of the grown films were determined by x-ray reflectometry (XRR) measurements performed using Cu-K_α (λ = 0.15406 nm) monochromatic radiation.

The mass densities were calculated by using the critical angle θ_c for the total external reflection [8]. The measured XRR curves were also fitted using simulated curves generated by using X'pert reflectivity program [22] to obtain the film thickness as well as to confirm the calculated mass densities. Elemental composition including the H content of the grown films was investigated by employing time-of-flight elastic recoil detection analysis (ToF-ERDA) using 32 MeV $^{127}I^{8+}$ beam. The ion incident angle relative to the surface normal was 67.5° and the detector was positioned at a recoil angle of 45°. A detailed description of the experimental set-up has been given elsewhere [23,24]. A reference sample with known H content was used for calibration of the data. Hardness of the films was measured by employing a nanoindenter (UMIS-2000, Fischer-Cripps Laboratories) where a Berkovich shaped diamond tip was used to obtain indentation data from which the hardness values were extracted using the Oliver-Pharr method [25].

B. SPECIFIC EXPERIMENTAL STRATEGY

The film growth was performed using two different discharge processes which are described as follows:

Discharge 1: This discharge was generated by superposing HiPIMS and DCMS using equal power fractions of a total of 50 W in an Ar:C_2H_2 ambient of 95% Ar and 5% C_2H_2. a-C:H films were grown under varied incident energies of the depositing species, E_{ion}. The advantage of using the superposition is that the DC-power maintains the plasma between the HiPIMS pulses providing stable operating conditions. The grown films are specified below as HiPIMS+DCMS: 5% C_2H_2.

Discharge 2: Increase of the HiPMS power fraction is known to lead to higher plasma densities and higher ion contents in the deposition flux [26]. Changes in the plasma density may also influence rates of interactions of energetic electrons with complex molecules (C_2H_2

in this case) and thereby affect the chemistry of the deposition flux. In order to investigate these relationships, this discharge was generated using a larger HiPIMS fraction (35 W HiPIMS and 15 W DC). In this case a lower C_2H_2 fraction of 2% was used. The films were grown by choosing the same E_{ion} as those used for the films grown using discharge 1. These films are denoted as HiPIMS+DCMS: 2% C_2H_2.

III. SIMULATIONS OF ION-FILM INTERACTIONS

In order to elucidate the interactions of relevant ionized species from the above mentioned plasma discharges with the films, Monte Carlo based computer simulations were performed using the TRIM software [21]. For these simulations, we consider ionized atomic species H^+, C^+ and Ar^+ because in our discharges, these ions along with the molecular hydrocarbon ions are the expected dominating species (see discussion in section V A). The molecular hydrocarbon ions such as $C_2H_2^+$ dissociate into atomic components at the impact to the surface [27] (also see discussion in section V B) therefore, their influence on the film growth are inferred by studying interaction of atomic C and H with the grown surfaces. E_{ion} was chosen as 15, 150 and 300 eV corresponding to V_{fl} and U_b values of 150 and 300 V, respectively, under the assumption of $E_{ion} = eU_b$, where e is the elementary charge. The initial kinetic energy of ions and collisions that they may undergo *en route* to the substrate were not taken into account for estimating the impingement energy. The film surface (C-H layer) was constructed using the experimentally determined structural properties of the films grown at $E_{ion} = -eV_{fl}$ from discharges 1 and 2. This includes the C and H contents as well as the mass densities of the films. The other layer properties such as the surface binding energy and displacement energy of the bonded C and H atoms into the film were taken from the TRIM software. Data were collected for the resulting depth distribution functions of the bombarding ions.

IV. RESULTS

The deposition rates of films grown using the discharge processes described in section II B are presented in Fig. 1. The rates are also compared with data from a HiPIMS discharge operated in 100% Ar ambient [18]. With reference to the pure Ar HiPIMS discharge, a substantial increase in the deposition rate is observed when 2% C_2H_2 is added to the HiPIMS+DCMS discharge. A slight further increase is achieved when the amount of C_2H_2 is increased from 2% to 5%, in which case the rate is 10 times larger than the value obtained from a HiPIMS discharge operated in 100% Ar ambient. The mass densities of the films from discharges 1 and 2 (section II B) as a function of E_{ion} are presented and compared with those of a 100% Ar HiPIMS discharge [18] in Fig. 2. The densities of the films from the two Ar-C_2H_2 superimposed discharges are similar with the 5% C_2H_2 discharge yielding higher values at relatively low E_{ion}. In both discharge conditions lower E_{ion} leads to the formation of low density phases of a-C:H, while a gradual increase in the densities is observed when increasing E_{ion}. Furthermore, the densities are lower at all E_{ion} values as compared to those obtained using 100% Ar HiPIMS discharge. Moreover, the optimum film densities are reached at much higher E_{ion} values (about two times) when C_2H_2 is added in the gas atmosphere. The H contents of the films from discharges 1 and 2 are compared in Fig.3. The general trend is the same for both of discharges, i.e., the H content decreases with increasing E_{ion}. Films grown using C_2H_2 fraction of 2% exhibit lower H contents as compared to the 5% case. The maximum H content (13.7%) is found in the film grown using 5% C_2H_2 at E_{ion} = – eV_{fl} while the minimum H content of 8.4% is obtained for the film grown using 2% C_2H_2 at E_{ion} corresponding to 300 eV. The common impurities such as O and N were found to be in negligibly small amounts into all grown films (not shown here). The same holds for the amount of incorporated Ar (~ 1% for E_{ion} of 300 eV). The hardness of the films (film thickness ≥1μm) grown using the two discharges employed in the present study are shown in

Fig.4. Both discharges yield similar results, i.e., the hardness is seen to increase from about 5 GP to over 25 GPa for E_{ion} increasing from $-eV_{fl}$ to 300 eV. Moreover, no appreciable difference between the hardness values for 2% and 5% C_2H_2 content is seen.

The simulated depth distribution functions of H^+, C^+ and Ar^+ ions for different E_{ion} are shown in Fig.5a and Fig.5b. C^+ ions exhibit a narrow distribution (Fig.5a) at E_{ion} corresponding to $-eV_{fl}$ where the penetration is limited to only about 1 nm below the surface. With increased E_{ion} (150 eV) they undergo a shallow implantation where most of the C^+ ions can penetrate up to about 2 nm, while the tail extends to about 4 nm beneath the surface. At E_{ion} = 300 eV, the distribution becomes broader and the penetration increases down to about 6 nm below the film surface. A comparison of the depth distributions for H^+, C^+ and Ar^+ ions for the E_{ion} of 300 eV is provided in Fig.5b. At this energy, the penetration of majority of Ar^+ ions is limited to about 2–3 nm below the surface. The same is true for the majority of C^+ ions with a small fraction of them reaching as deep as about 6 nm. In comparison, the H^+ ions penetrate to substantially higher depths than Ar^+ and C^+ ions (the tail is extending to about 20 nm) with an average penetration depth of approximately 10 nm.

V. DISCUSSION

A. PLASMA CHEMISTRY

The plasma chemistry in high density discharges that contain a hydrocarbon gas is mainly driven by electron impact induced reactions such as dissociation, excitation and ionization of the precursor gas molecules [19,28,29], see Table I. Depending on plasma energetics and energy thresholds of the various reactions, different types of ionized species, such as $C_2H_2^+$, C_2H^+, C^+, H^+ as well as neutral radicals, such as C_2H and CH can be generated [19,30]. These species may constitute film forming flux, depending on their reactivity, surface loss probability and residence time in the plasma [30,31]. The formation of C_2H radicals via

dissociation has the lowest energy threshold (~ 7.5 eV) [29] and therefore, a very high probability for the reaction is expected. The C_2H radicals are highly reactive and possess a very high surface loss probability [13,32]. Therefore, they take part in the polymerization of parent C_2H_2 molecules leading to the long-chained poly-acetylene molecules $(C_2H_2)_n$ (n = 1,2,3…) [19] as well as they are lost to the surfaces in the chamber. Doyle *et al.* [30] and Baby *et al.* [33] concluded via experimental investigations and modeled reaction mechanisms that for the diamond-like hydrogenated carbon (DLC:H) growth using C_2H_2 precursor in RF-PECVD and ICP discharges, the C_2H radical is the dominating film forming species. On the other hand, in the plasma based discharges where the ionized fraction of the depositing fluxes reaches close to 100%, $C_2H_2^+$ and C_2H^+ ions have been identified as the dominating film forming species [27]. In our case of Ar/C_2H_2-based HiPIMS+DCMS discharge operating at low pressure and high electron density, ionization of sputtered C may also be an important plasma phase reaction [18]. Thus, C containing sputtered and hydrocarbon species (C, C^+, C_2H, C_2H^+, C_2H_2, $C_2H_2^+$) are likely to be the main constituents of the deposition fluxes. It should be also noted that atomic H is the product specie from several of these reactions listed in Table I, i.e., the discharge employed in the present study is likely to contain large amounts of H including both, neutral and ionized in accordance with previous literature reports [19,30,33]. Moreover, owing to the fact that Ar content in the HiPIMS+DCMS discharges is more than 95%, it should be expected that there is a considerable flux of Ar^+ ions towards the growing film.

The neutral and ionized hydrocarbon species present in our discharge are an additional source of C which explains the increase of film growth rate as compared to the Ar-HiPIMS discharge (see Fig. 1) where the only source of film forming species is sputtered C. The role of hydrocarbon species as additional C source is further manifested by the increase of the film growth rate when the C_2H_2 content is increased from 2 to 5% (Fig. 1). However, the

difference in the film growth rate between HiPIMS+DCMS: 5% C_2H_2 and HiPIMS+DCMS: 2% C_2H_2 discharges is not as pronounced as the difference observed between the later discharge and the HiPIMS: 100% Ar conditions. This may be an effect of a higher amount of C_2H_2 which may cool down the electrons leading to a lower rate of dissociation and ionization of the precursor gas. A lower HiPIMS fraction used in this case will also contribute to a lower rate of dissociation and ionization.

B. FILM GROWTH

Besides the arrival rate of film forming species, the film growth is also affected by the energy with which these species reach the substrate. The sputtered neutral C atoms and C^+ ions with relatively low E_{ion} arrive at the film surface and form mainly sp^2 coordinated bonds with the surface C atoms. Similarly the incoming hydrocarbon neutrals and ions with relatively low E_{ion} get physisorbed or chemisorb to active sites on the film surface, most commonly to a dangling bond [28,31]. Thus, their contribution to film growth depends on their sticking coefficient and surface dangling bond density [28,31]. Closed shell radicals such as C_2H_2 have very low sticking coefficients whereas unsaturated radicals such as C_2H exhibit very high sticking coefficients (close to 1) [32,34]. The surface dangling bond density depends on the abstraction of surface bonded H (cross-section, $\sigma_{\text{abstraction, H}} \sim 0.05$ Å^2) [34] by the incoming species however, at no or low energetic bombardment conditions (e.g., at $E_{ion} = -eV_{fl}$), the H from the discharge quickly saturates the created dangling bonds (cross-section, $\sigma_{\text{addition, H}} \sim 1.3$ Å^2) [34]. Therefore under these conditions, mainly unsaturated radicals contribute to the film growth. At the surface, these radicals undergo a bond rearrangement where the constituting C atoms enter into either C-C sp^2 coordinated bonds or C-H sp^3 bonds [32]. Overall, under low energetic bombardment conditions the sp^2 rich a-C growth pursues. This together with a substantial amount of H incorporation results in the a-C films which exhibit a low density [5,35]. For example, Godet *et al.* [36] showed that polymeric a-C:H

films exhibiting low mass densities (< 2 g/cm^3) and high H content (25%–40%) are grown under low RF bias powers using C_2H_2 as well as CH_4 based ECR discharges while Baby *et al.* [37] found a high average Raman base line slope at lower substrate bias potentials which corresponds to a high H content in the films when they deposited a-C:H films using C_2H_2/Ar based ICP discharge. In our case similar trends with respect to mass density are observed for films (see Fig.2) grown using HiPIMS+DCMS at $E_{ion} = -eV_{fl}$, whereas in 100% Ar HiPIMS case (where there is no intentional use of H) the film exhibit higher density at this ion energy values.

The growth conditions change when E_{ion} is raised to a level where it exceeds the surface penetration threshold energy, E_p (32 eV for a graphite surface) [5,38]. In this case, the ions penetrate through the surface and are implanted into subsurface regions (see Fig.5a). For single carbon species such as C^+ ions, $E_{ion} \sim eU_b$ therefore they are likely to be implanted for U_b value of 32 V and higher. The ionized species with two or more C atoms such as $C_2H_2^+$, tend to split upon their impact at the surface [27] therefore, E_{ion} in this case is shared among the constituents. In order to determine if the implantation of a daughter C atoms takes place, the energy per deposited C atom, E_C, should be calculated. For example, for $C_2H_2^+$ ions E_C can be calculated as,

$$E_c = \frac{m_c E_{ion}}{2m_c + 2m_H} \qquad (1)$$

where m_C and m_H are the masses of C and H atoms, respectively. For these ions, U_b of about 70 V is required for E_C to become equal to E_p.

As a result of implantation, an increase in the local density of C atoms in the subsurface region occurs which causes a bond rearrangement from weaker C-C sp^2 to stronger C-C sp^3 bonds giving rise to denser phase of a-C as compared to the growth with lower E_{ion} than E_p [5,38]. A further increase in E_{ion} is likely to enhance implantation which in turn would result

in an increased mass density of the film. This has been demonstrated by Weiler *et al.* [27] for ta-C:H films grown using a C_2H_2 based plasma beam where an increase in energy per deposited C atom resulted in an increase in the mass density as well as C-C sp^3 bond fraction of the films. This is also evident in Fig.2 where for discharge conditions an increase in the mass density of the films is observed when E_{ion} is increased. The mass densities of the films using HiPIMS+DCMS discharges reach saturation at higher values of E_{ion} as compared to the HiPIMS: 100% Ar. This fact indicates that the film growth in the former case is dominated by ionized hydrocarbon species where two or more C atoms are present and share E_{ion} upon impacting the surface of the growing film according to Eq. (1). The lower mass densities using the C_2H_2 containing discharges as compared to 100% Ar HiPIMS may be attributed to the difference in the amount of incorporated H.

As discussed in section V A, Ar^+ and H^+ ions are also present during film growth. Ar^+ ions do not penetrate deep into the film even at high E_{ion} as it is seen in Fig.5b, which is in agreement with the ERDA measurements and they may contribute to the film densification via knock-on implantation of surface C atoms at relatively high E_{ion} [5,6,39]. H^+ ions on the other hand being much smaller in mass do not transfer appreciable momentum to C atoms, i.e., they cannot induce film densification via the pathways described in the previous paragraphs. However, owing to their small size H^+ ions can penetrate to large depths [35], especially at relatively high E_{ion} as seen in Fig.5b, bringing about other structural changes in the film. H^+ ions bombarding the growing film surface increase the dangling bond density by removing surface bonded H and give rise to higher chemisorption of the arriving hydrocarbon species [32]. In subsurface regions, they impart large fraction of their energy to displace the bonded H. Bonded H can also be displaced by the C^+ ion implantation [31,34] especially at higher E_{ion}, where C^+ ions penetrate deeper into subsurface region (see Fig.5a) and possess much higher energy than the displacement threshold of bonded H (~ 3 eV) [5]. The displaced H can

form H_2 molecule that diffuse to the surface thereby desorbing into the plasma [32,34,40]. This mechanism of H removal is most likely governing the decrease in the H content of the films with increased E_{ion} (see Fig.3). A decrease in the amount of H with increased E_{ion} can also affect the bonding configuration causing bond rearrangement where C-H bonds are replaced by C-C bonds. The increased number of C-C bonds give rise to an increase in the density as well as the hardness of the film is also increased [5] which can explain the findings in Figs. 2 and 4.

VI. SUMMARY

We have compiled and implemented a sputtering-based synthesis route for synthesis of hydrogenated amorphous carbon (a-C:H) thin films that entails coupling a hydrocarbon gas (acetylene) with high density discharges generated by the superposition HiPIMS and DCMS. We have tuned discharge density, gas phase composition and energy of the ionized depositing species and achieved conditions capable of providing ten-fold increase in the deposition rate of a-C:H films growth compared to HiPIMS Ar discharge [18]. This has been achieved without severely compromising density, hardness and H content of the resulting films. The achieved mass densities along with the high hardness values entail improved film properties as compared to those obtained using RF-PECVD and ICP-PECVD methods [37,41]. Using our experimental data in combination with Monte-Carlo computer simulations and literature data we have suggested that: (i) dissociative reactions triggered by the interactions of energetic discharge electrons with hydrocarbon gas molecules is an important additional (to the sputtering cathode) source of film forming species and (ii) film microstructure and film hydrogen content are primarily controlled by interactions of energetic plasma species with surface and sub-surface layers of the growing film. This notion may be of relevance for designing sputtering-based routes for high rate synthesis of hard and dense a-C:H films.

ACKOWLEDGEMENTS

AA and UH gratefully acknowledge the financial support provided by the Swedish Research Council (VR) through the contract 621-2011-4280. K.S. should like to acknowledge financial support from Linköping University through the "*LiU Research Fellows*" program. The authors are also grateful for access to the Tandem Laboratory at Uppsala University. European Collaboration in Science and Technology (COST Action MP0804) is gratefully acknowledged for stimulating discussions.

VII. REFERENCES

[1] C. Casiraghi, J. Robertson, A.C. Ferrari, Diamond-like carbon for data and beer storage Carbon is a very versatile element that can crystallize in the forms of, Rev. Lit. Arts Am. 10 (2007) 44–53.

[2] G. Dearnaley, J.H. Arps, Biomedical applications of diamond-like carbon (DLC) coatings: A review, Surf. Coatings Technol. 200 (2005) 2518–2524.

[3] J.K. Luo, Y.Q. Fu, H.R. Le, J.A. Williams, S.M. Spearing, W.I. Milne, Diamond and diamond-like carbon MEMS, J. Micromechanics Microengineering. 17 (2007) S147–S163.

[4] M. Chhowalla, J. Robertson, C.W. Chen, S.R.P. Silva, C.A. Davis, G.A. J. Amaratunga, W.I. Milne, Influence of ion energy and substrate temperature on the optical and electronic properties of tetrahedral amorphous carbon (ta-C) films, J. Appl. Phys. 81 (1997) 139–145.

[5] J. Robertson, Diamond-like amorphous carbon, Mater. Sci. Eng. R Reports. 37 (2002) 129–281.

[6] S. Logothetidis, C. Charitidis, P. Patsalas, Engineering properties of fully sp^3-to-sp^2 bonded carbon films and their modifications after post-growth ion irradiation, Diam. Relat. Mater. 11 (2002) 1095–1099.

[7] C.A. Charitidis, Nanomechanical and nanotribological properties of carbon-based thin films: A review, Int. J. Refract. Met. Hard Mater. 28 (2010) 51–70.

[8] A.C. Ferrari, A. Libassi, B.K. Tanner, V. Stolojan, J. Yuan, L.M. Brown, S.E. Rodil, B. Kleinsorge, J. Robertson, Density, sp^3 fraction, and cross-sectional structure of amorphous carbon films determined by x-ray reflectivity and electron energy-loss spectroscopy, Phys. Rev. B. 62 (2000) 11089–11103.

[9] P.J.U. Martin, A. Bendavid, Review of the filtered vacuum arc process and materials deposition, Thin Solid Films. 394 (2001) 1–15.

[10] P. Patsalas, S. Kaziannis, C. Kosmidis, D. Papadimitriou, G. Abadias, G. A. Evangelakis, Optimized pulsed laser deposition by wavelength and static electric field control: The case of tetrahedral amorphous carbon films, J. Appl. Phys. 101 (2007) 124903.

[11] A.A. Voevodin, M.S. Donley, Preparation of amorphous diamond-like carbon by pulsed laser deposition : a critical review, Surf. Coatings Technol. 82 (1996) 199–213.

[12] Y. Wang, H. Li, L. Ji, F. Zhao, X. Liu, Q. Kong, Y. Wang, W. Quan, H. Zhou, J. Chen, The effect of duty cycle on the microstructure and properties of graphite-like amorphous carbon films prepared by unbalanced magnetron sputtering, J. Phys. D. Appl. Phys. 43 (2010) 505401.

[13] D. Liu, J. Zhang, Y. Liu, J. Xu, G. Benstetter, Growth processes and surface properties of diamondlike carbon films, J. Appl. Phys. 97 (2005) 104901.

[14] J. Hopwood, Ionized physical vapor deposition of integrated circuit interconnects, Phys. Plasmas. 5 (1998) 1624.

[15] U. Helmersson, M. Lattemann, J. Bohlmark, A.P. Ehiasarian, J.T. Gudmundsson, Ionized physical vapor deposition (IPVD): A review of technology and applications, Thin Solid Films. 513 (2006) 1–24.

[16] K. Sarakinos, A. Braun, C. Zilkens, S. Mráz, J.M. Schneider, H. Zoubos, P. Patsalas, Exploring the potential of high power impulse magnetron sputtering for growth of diamond-like carbon films, Surf. Coatings Technol. 206 (2012) 2706–2710.

[17] B.M. Dekoven, P.R. Ward, R.E. Weiss, S. Clara, D.J. Christie, R.A. Scholl, W.D. Sproul, F. Tomasel, A. Anders, Carbon Thin Film Deposition Using High Power Pulsed Magnetron Sputtering, 46th Annu. Tech. Conf. Proc. (2003) 158–165.

[18] A. Aijaz, K. Sarakinos, D. Lundin, N. Brenning, U. Helmersson, A strategy for increased carbon ionization in magnetron sputtering discharges, Diam. Relat. Mater. 23 (2012) 1–4.

[19] J. Benedikt, Plasma-chemical reactions: low pressure acetylene plasmas, J. Phys. D. Appl. Phys. 43 (2010) 043001.

[20] J. Benedikt, R.V. Woen, S.L.M. Van Mensfoort, V. Perina, J. Hong, M.C.M. Van De Sanden, Plasma chemistry during the deposition of a-C : H films and its influence on film properties, Diam. Relat. Mater. 12 (2003) 90–97.

[21] J. F. Ziegler, “The stopping and range of ions in matter,” http://www.srim.org/, accessed January, 2013.

[22] Philips X’PERT Reflectivity (The Netherlands: PANalytical B. V.).

[23] H.J. Whitlow, G. Possnert, C.S. Petersson, Quantitative mass and energy dispersive elastic recoil spectrometry: Resolution and efficiency considerations, Nucl. Instruments and Methods Phys. Res. B 27 (1987) 448–457.

[24] J. Jensen, D. Martin, A. Surpi, T. Kubart, ERD analysis and modification of TiO_2 thin films with heavy ions, Nucl. Instruments Methods Phys. Res. B 268 (2010) 1893–1898.

[25] W.C. Oliver, G.M. Pharr, An improved technique for determining hardness and elastic modulus using load and displacement sensing indentation experiments, J. Mater. Res. 7 (1992) 1564–1583.

[26] M. Samuelsson, D. Lundin, K. Sarakinos, F. Björefors, B. Wälivaara, H. Ljungcrantz, U. Helmersson, Influence of ionization degree on film properties when using high power impulse magnetron sputtering, J. Vac. Sci. Technol. A Vacuum, Surfaces, Film. 30 (2012) 031507.

[27] M. Weiler, S. Sattel, T. Giessen, K. Jung, H. Ehrhardt, Preparations and properties of highly tetrahedral hydrogenated amorphous carbon, Phys. Rev. B 53 (1996) 1594–1608.

[28] Y.H. Cheng, Y.P. Wu, J.G. Chen, X.L. Qiao, C.S. Xie, B.K. Tay, S.P. Lau, X. Shi, On the deposition mechanism of a-C:H films by plasma enhanced chemical vapor deposition, Surf. Coatings Technol. 135 (2000) 27–33.

[29] K. De Bleecker, A. Bogaerts, W. Goedheer, Detailed modeling of hydrocarbon nanoparticle nucleation in acetylene discharges, Phys. Rev. E. 73 (2006) 026405.

[30] J.R. Doyle, Chemical kinetics in low pressure acetylene radio frequency glow discharges, J. Appl. Phys. 82 (1997) 4763.

[31] C. Lopez-Santos, J.L. Colaux, J.C. Gonzalez, S. Lucas, Investigation of the Growth Mechanisms of a-CHx Coatings Deposited by Pulsed Reactive Magnetron Sputtering, J. Phys. Chem. C. 116 (2012) 12017–12026.

[32] W. Jacob, Surface reactions during growth and erosion of hydrocarbon films, Thin Solid Films. 326 (1998) 1–42.

[33] A. Baby, C.M.O. Mahony, P.D. Maguire, Acetylene–argon plasmas measured at a biased substrate electrode for diamond-like carbon deposition: I. Mass spectrometry, Plasma Sources Sci. Technol. 20 (2011) 015003.

[34] A. von Keudell, M. Meier, C. Hopf, Growth mechanism of amorphous hydrogenated carbon, Diam. Relat. Mater. 11 (2002) 969–975.

[35] J. Robertson, Deposition mechanism of a-C and a-C:H, J. Non. Cryst. Solids. 164-166 (1993) 1115–1118.

[36] C. Godet, N.M.J. Conway, J.E. Bourée, K. Bouamra, A. Grosman, C. Ortega, Structural and electronic properties of electron cyclotron resonance plasma deposited hydrogenated amorphous carbon and carbon nitride films, J. Appl. Phys. 91 (2002) 4154.

[37] A. Baby, C.M.O. Mahony, P. Lemoine, P.D. Maguire, Acetylene–argon plasmas measured at an rf-biased substrate electrode for diamond-like carbon deposition: II. Ion energy distributions, Plasma Sources Sci. Technol. 20 (2011) 015004.

[38] H. Jäger, A. Belov, ta-C deposition simulations: Film properties and time-resolved dynamics of film formation, Phys. Rev. B. 68 (2003) 024201.

[39] P. Patsalas, S. Logothetidis, The effect of postgrowth ion irradiation on the microstructure and the interface properties of amorphous carbon films on silicon, J. Appl. Phys. 88 (2000) 6346–6354.

[40] A. von Keudell, Formation of polymer-like hydrocarbon films from radical beams of methyl and atomic hydrogen, Thin Solid Films. 402 (2002) 1–37.

[41] P. Koidl, C. Wild, B. Dischler, J. Wagner, M. Ramsteiner, Plasma Deposition, Properties and Structure of Amorphous Hydrogenated Carbon Films, Mater. Sci. Forum. 52-53 (1990) 41–70.

FIGURE CAPTIONS

FIG. 1. The normalized deposition rates per Watt for the film growth using different processes. The deposition rates are normalized to pure HiPIMS in 100% Ar process [18]. The actual deposition rates are ~ 2 nm/min (at 42 W), ~ 18.5 nm/min (at 50 W) and ~ 25 nm/min (at 50 W) for HiPIMS: 100% Ar, HiPIMS+DCMS: 2% C_2H_2 and HiPIMS+DCMS: 5% C_2H_2 respectively.

FIG. 2. Comparison of the mass densities of HiPIMS+DCMS: 5% C_2H_2 grown a-C:H films with the mass densities of HiPIMS+DCMS: 2% C_2H_2 as well as with previously grown HiPIMS: 100% Ar films [18]. A maximum error of 2% in mass densities was found during mass density determination using the curve fitting.

FIG. 3. H content as a function of the substrate bias potential/ion energy for a-C:H films grown using HiPIMS+DCMS: 5% C_2H_2 and HiPIMS+DCMS: 2% C_2H_2 processes at 2 Pa of operating pressure and 50 W of average power. An error ranging from 0.92% to 1.1 at. % was found in determining the H-contents.

FIG. 4. Hardness as a function of substrate bias potential/ion energy of the a-C:H films synthesized using HiPIMS+DCMS: 5% C_2H_2 and HiPIMS+DCMS: 2% C_2H_2 processes at 2 Pa of operating pressure and an average power of 50 W. The error in the hardness values was found not to exceed 4%.

FIG. 5. Simulated depth distribution functions for (a) C^+ ions with E_{ion} of $-eV_{fl}$, 150 eV and 300 eV and (b) Ar^+, C^+ and H^+ ions with E_{ion} of 300 eV, bombarding a C-H layer of mass density 1.621 g/cm^3 and H content of 12.3%. The C-H layer is the replica of the film deposited using HiPIMS+DCMS: 2% C_2H_2 process at 2 Pa of operating pressure and $E_{ion} = -eV_{fl}$ using an average power of 50 W.

FIG. 1

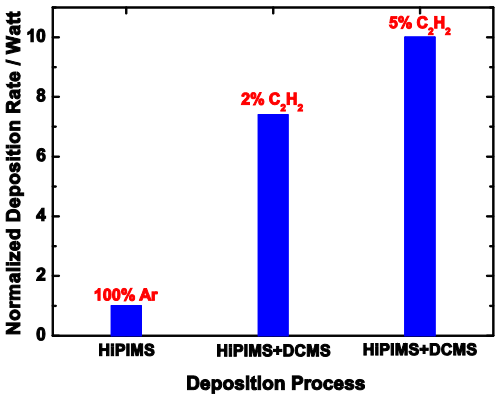
Normalized Deposition Rate / Watt
0
2
4
6
8
10
100% Ar
2% C2H2
5% C2H2
HIPIMS
HIPIMS+DCMS
HIPIMS+DCMS
Deposition Process

FIG. 2

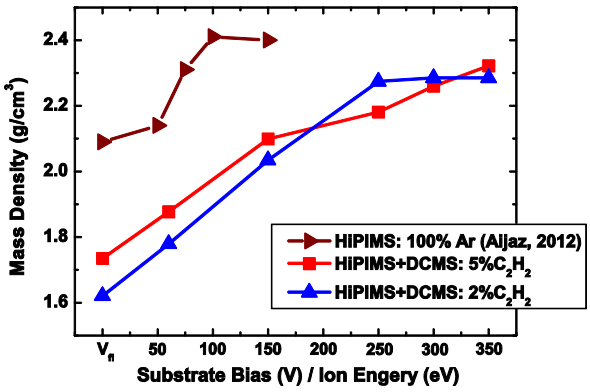
Mass Density (g/cm3)
1.6
1.8
2.0
2.2
2.4
Vfl
50
100
150
200
250
300
350
Substrate Bias (V) / Ion Engery (eV)
HIPIMS: 100% Ar (Aljaz, 2012)
HIPIMS+DCMS: 5%C2H2
HIPIMS+DCMS: 2%C2H2

FIG. 3

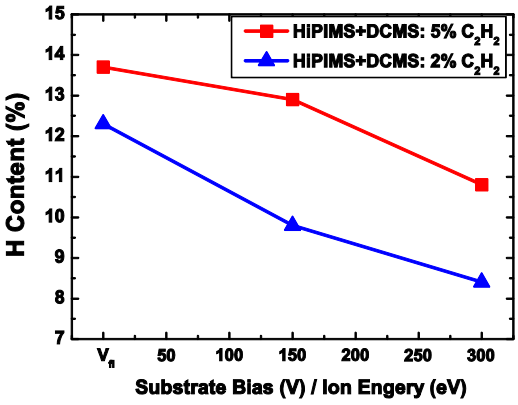
HiPIMS+DCMS: 5% C2H2
HiPIMS+DCMS: 2% C2H2
H Content (%)
15
14
13
12
11
10
9
8
7
Vf
50
100
150
200
250
300
Substrate Bias (V) / Ion Engery (eV)

FIG. 4

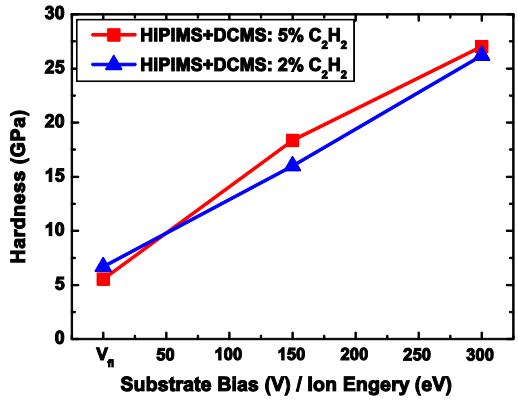
HiPIMS+DCMS: 5% C2H2
HiPIMS+DCMS: 2% C2H2
Hardness (GPa)
30
25
20
15
10
5
0
Vf
50
100
150
200
250
300
Substrate Bias (V) / Ion Engery (eV)

FIG. 5

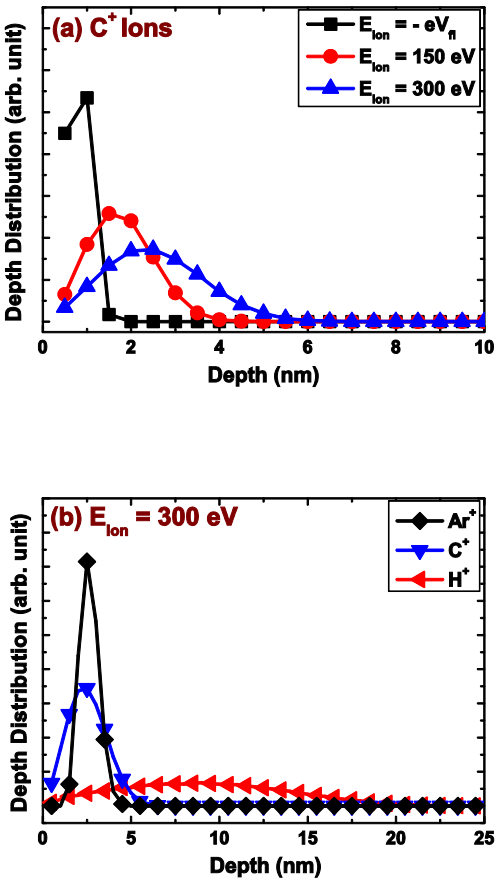
(a) C+ Ions
E_Ion = - eV_fl
E_Ion = 150 eV
E_Ion = 300 eV
Depth Distribution (arb. unit)
Depth (nm)
0
2
4
6
8
10
(b) E_Ion = 300 eV
Ar+
C+
H+
Depth Distribution (arb. unit)
Depth (nm)
0
5
10
15
20
25

Table I: Commonly observed electron impact induced reactions along with their threshold energies in low-pressure C_2H_2 containing plasma discharges [29] (and references therein). The first ionization thresholds for Ar, C and H are 15.75, 11.26 and 13.59 eV, respectively.

Reaction	Threshold Energy (eV)	Type of Reaction
$C_2H_2 + e^- \rightarrow C_2H + H + e^-$	7.5	Dissociation
$C_2H_2 + e^- \rightarrow C_2H_2^+ + 2e^-$	11.4	Ionization
$C_2H_2 + e^- \rightarrow C_2H^+ + H + 2e^-$	16.5	Dissociative Ionization
$C_2H_2 + e^- \rightarrow C_2^+ + H_2 + 2e^-$	17.5	Dissociative Ionization
$C_2H_2 + e^- \rightarrow H^+ + C_2H + 2e^-$	18.4	Dissociative Ionization
$C_2H_2 + e^- \rightarrow C^+ + CH_2 + 2e^-$	20.3	Dissociative Ionization
$C_2H_2 + e^- \rightarrow CH^+ + CH + 2e^-$	20.6	Dissociative Ionization

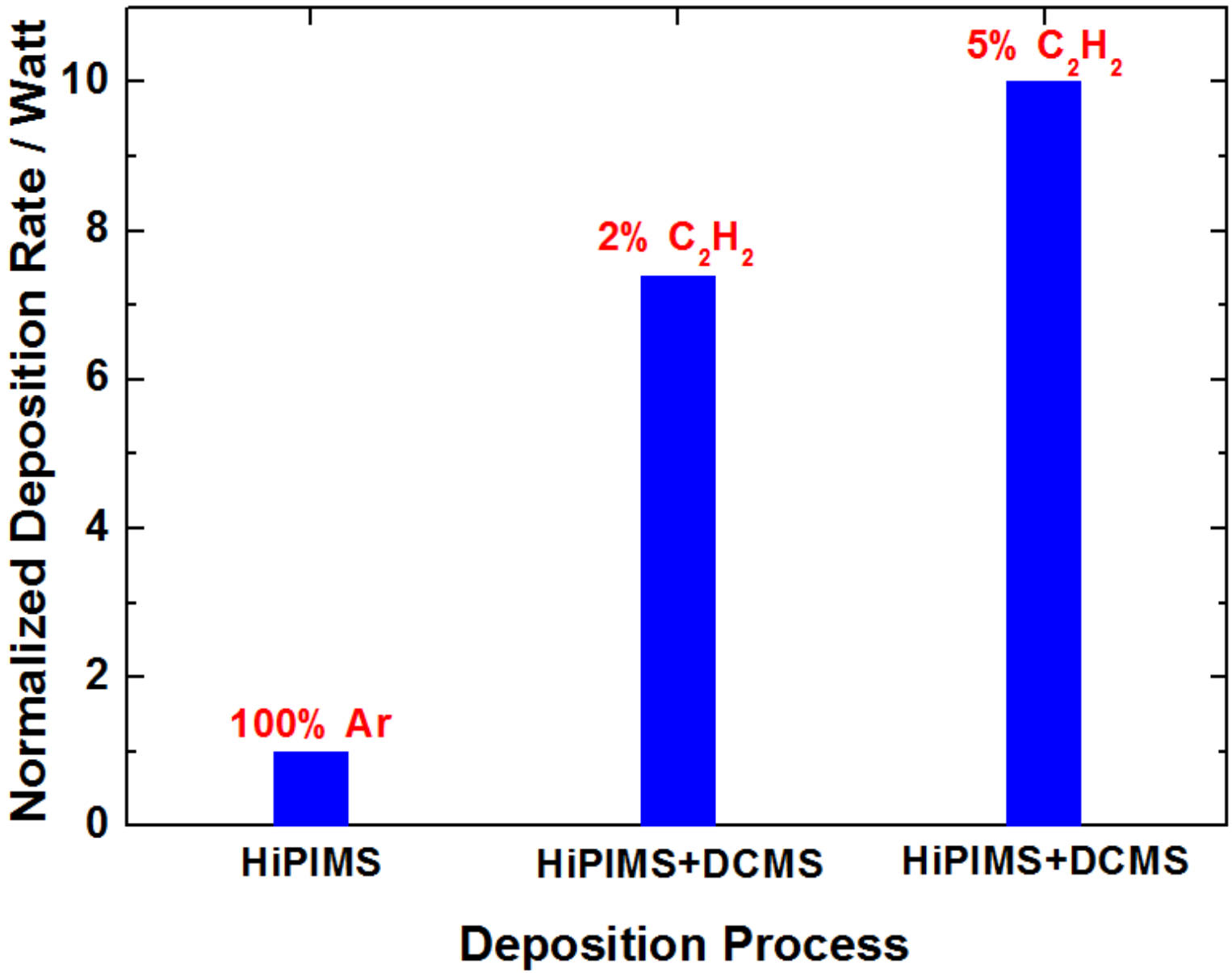
Normalized Deposition Rate / Watt
0
2
4
6
8
10
100% Ar
2% C2H2
5% C2H2
HiPIMS
HiPIMS+DCMS
HiPIMS+DCMS
Deposition Process

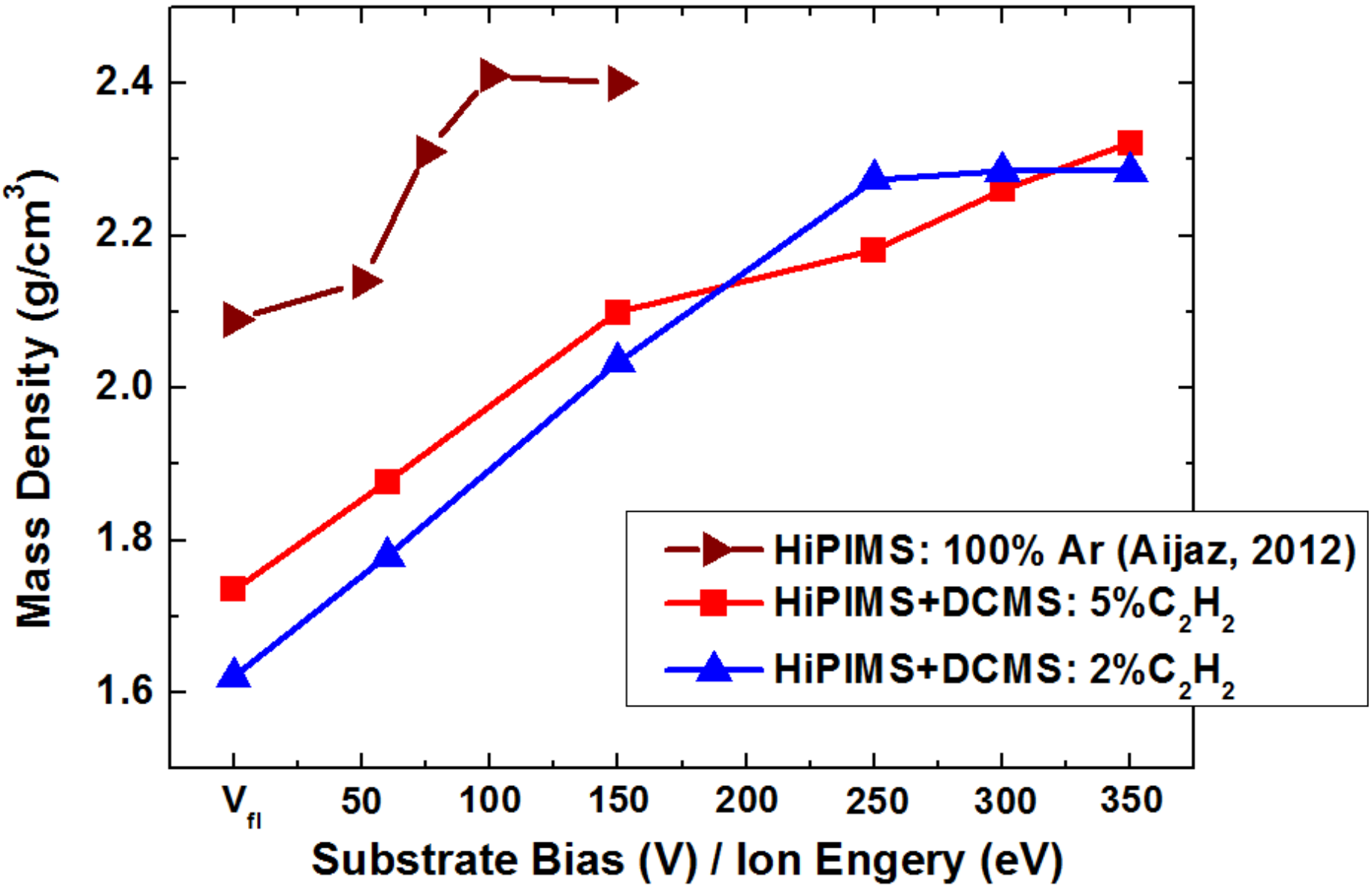
Mass Density (g/cm^3)
2.4
2.2
2.0
1.8
1.6
V_{fl}
50
100
150
200
250
300
350
Substrate Bias (V) / Ion Engery (eV)
HiPIMS: 100% Ar (Aijaz, 2012)
HiPIMS+DCMS: 5%C_2H_2
HiPIMS+DCMS: 2%C_2H_2

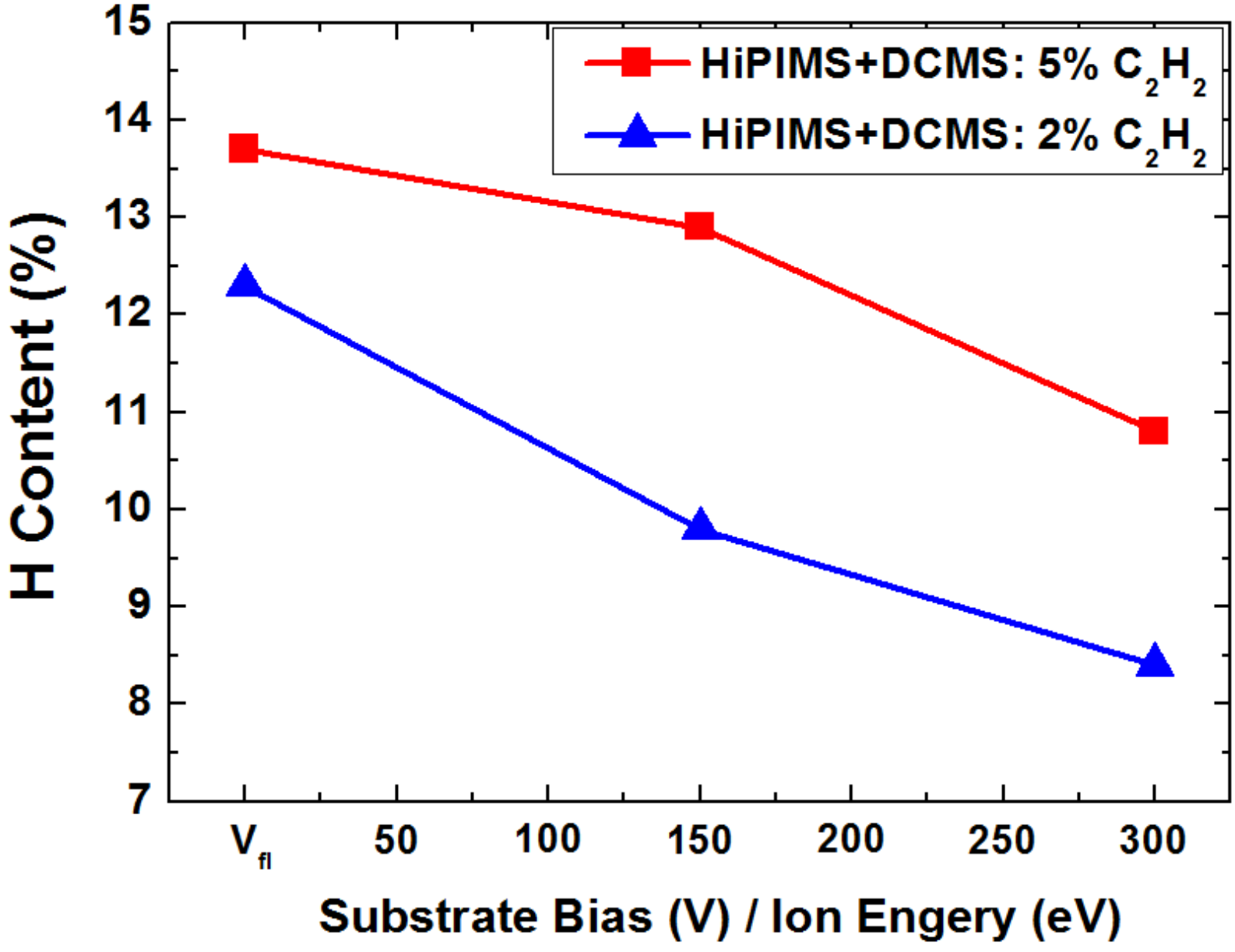
H Content (%)
15
14
13
12
11
10
9
8
7
HiPIMS+DCMS: 5% C2H2
HiPIMS+DCMS: 2% C2H2
Vfl
50
100
150
200
250
300
Substrate Bias (V) / Ion Engery (eV)

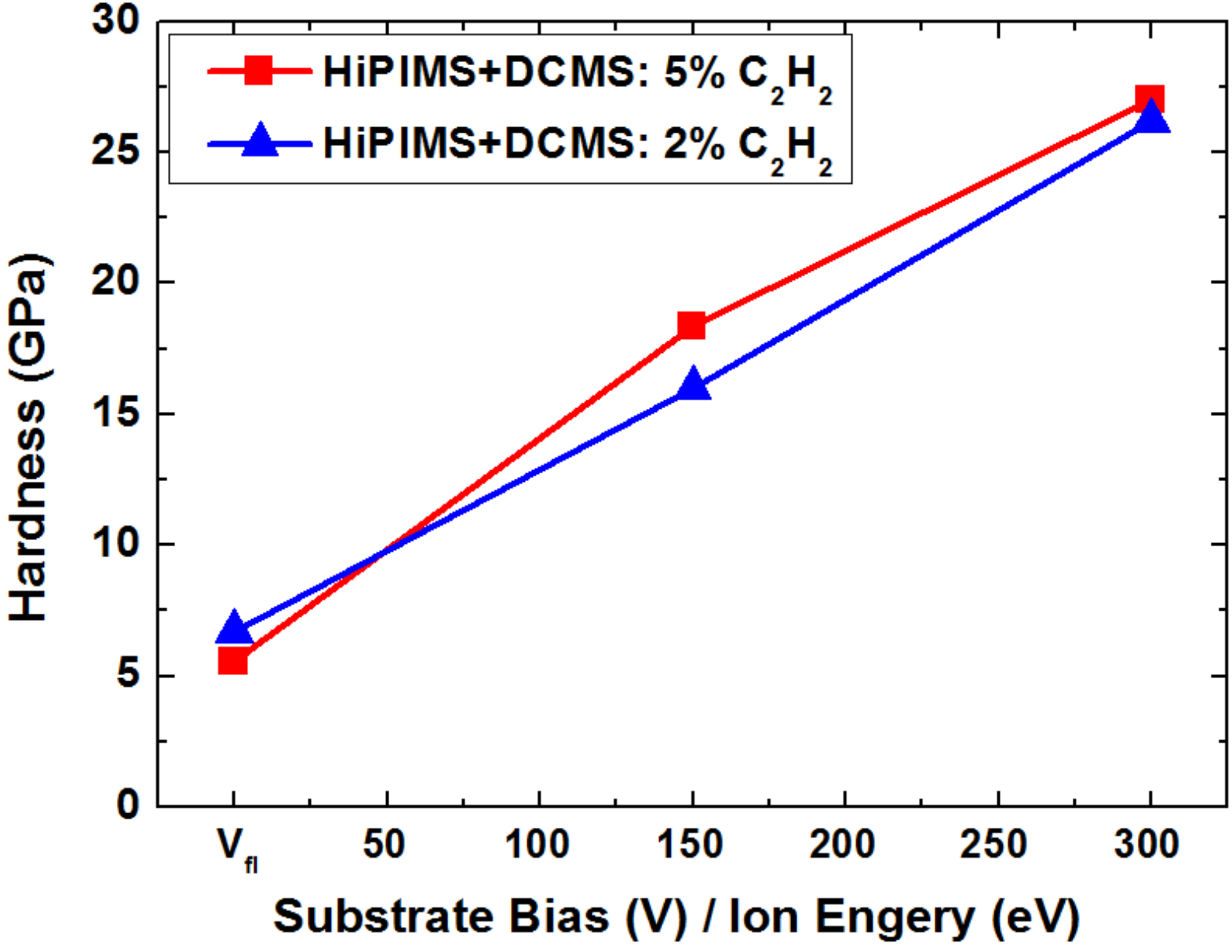
HiPIMS+DCMS: 5% C2H2
HiPIMS+DCMS: 2% C2H2
Hardness (GPa)
0
5
10
15
20
25
30
Vfl
50
100
150
200
250
300
Substrate Bias (V) / Ion Engery (eV)

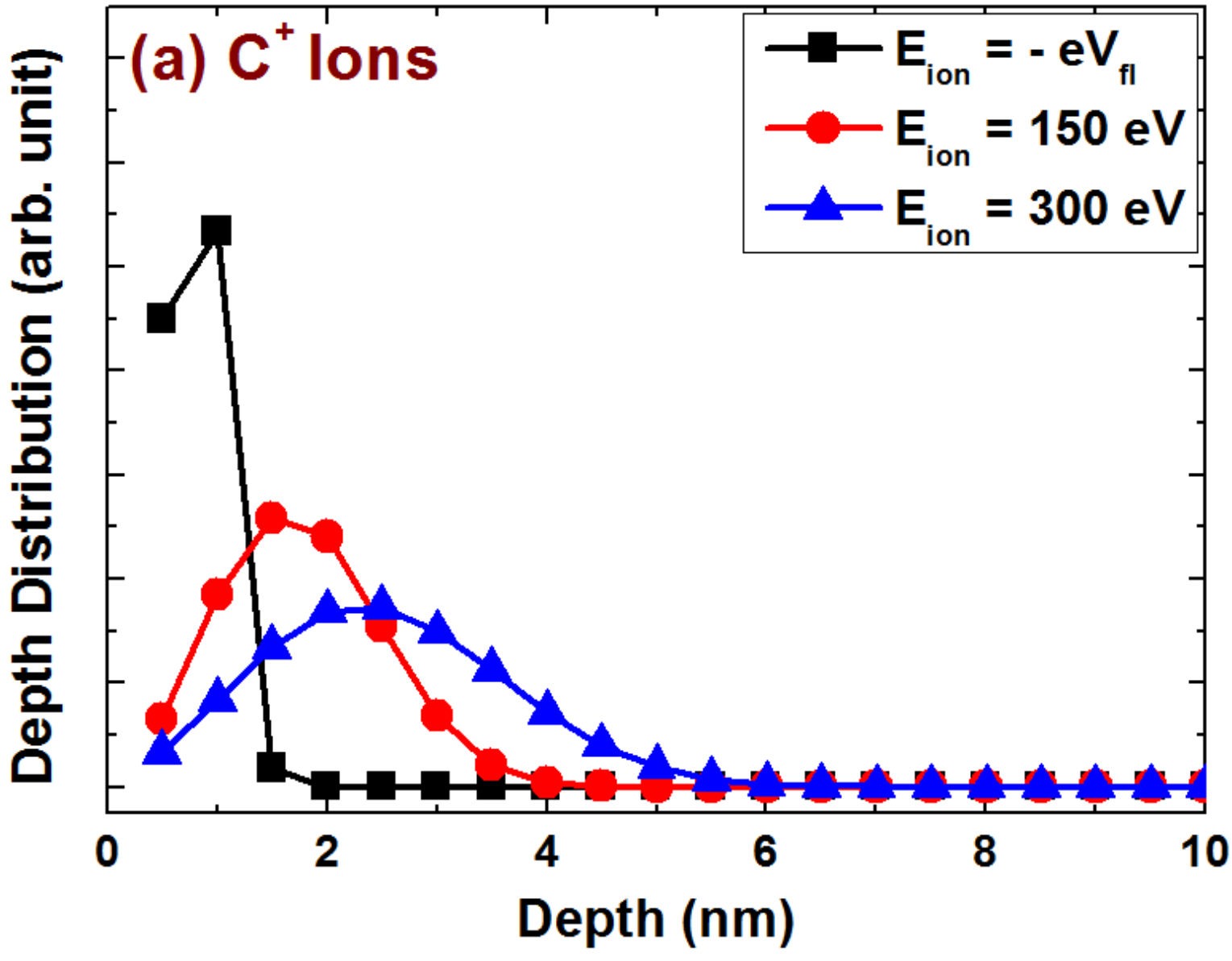
(a) C+ Ions
E ion = - eV fl
E ion = 150 eV
E ion = 300 eV
Depth Distribution (arb. unit)
0
2
4
6
8
10
Depth (nm)

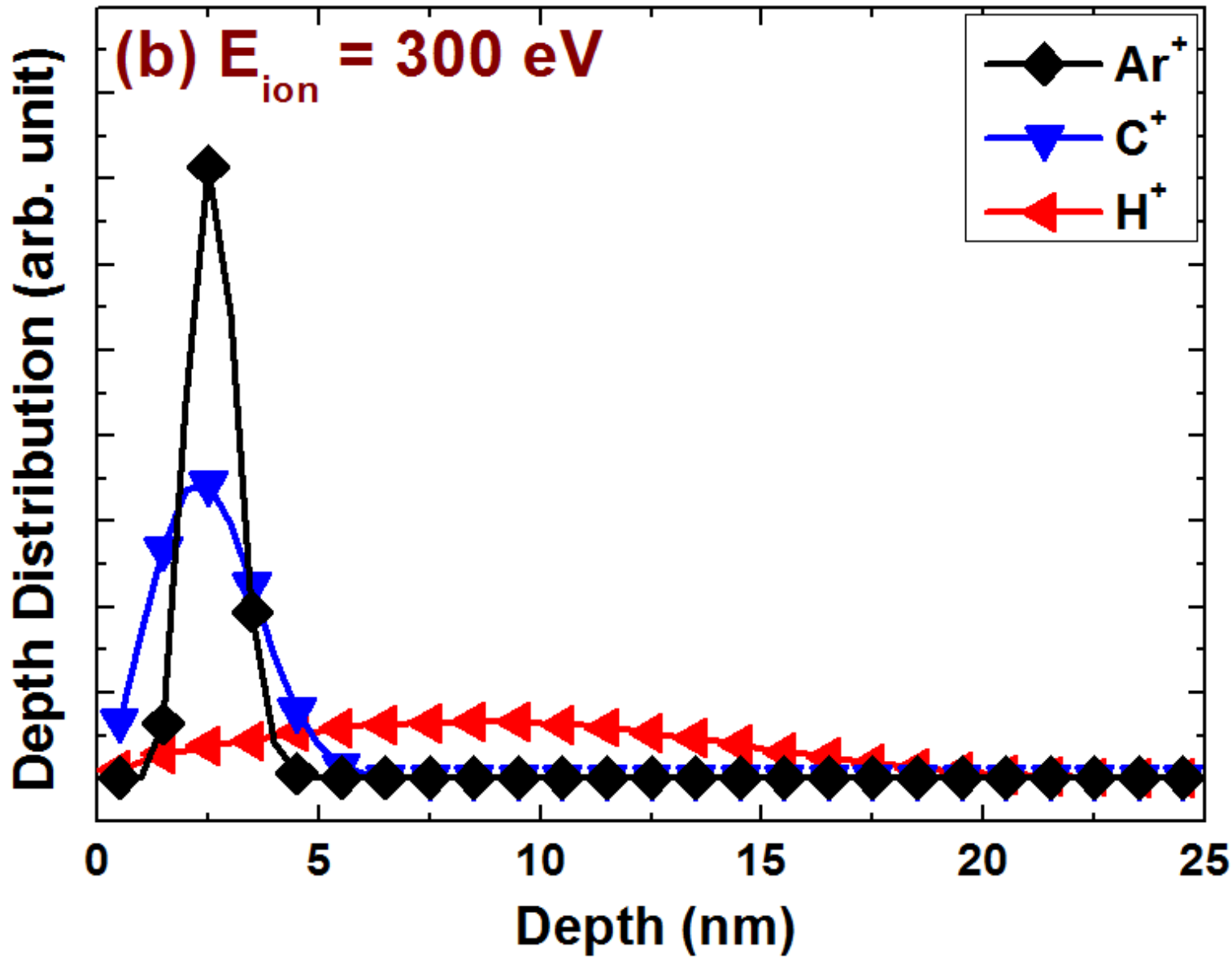
(b) E ion = 300 eV
Ar+
C+
H+
Depth Distribution (arb. unit)
0
5
10
15
20
25
Depth (nm)